ADDRESSABLE PLASMA PHOTONIC CRYSTALS

BY

HEE JUN YANG

THESIS

Submitted in partial fulfillment of the requirements
for the degree of Master of Science in Electrical and Computer Engineering
in the Graduate College of the
University of Illinois at Urbana-Champaign, 2015

Urbana, Illinois

Adviser:

Professor J. Gary Eden

ABSTRACT

Photonic crystals that comprise arrays of microplasmas can act as reconfigurable filters in the microwave and THz spectral regions. When compared to conventional photonic crystals fabricated in a solid, plasma photonic crystals are reconfigurable at electronic speeds which, in turn, allows for the transmission characteristics to be altered rapidly. This thesis will describe the theory and characteristics of photonic crystals, and the design and performance of photonic crystals based on arrays of microplasma jets will be discussed.

To my family, for their love and support.

ACKNOWLEDGMENTS

I am most grateful to my adviser, Professor J. Gary Eden, for his support, guidance, and advice in my research. Special thanks to Professor Sung-Jin Park, who shared brilliant ideas and guided my academic pathways since my undergraduate studies. Also, I would like to give thanks to all members of Laboratory for Optical Physics and Engineering (LOPE) for discussion and help for this thesis. Lastly, I would like to give my biggest thanks to my family for their support.

TABLE OF CONTENTS

CHAPTER 1

INTRODUCTION

Photonic crystals comprise a dielectric medium, composed of two or more materials, in which the refractive index is spatially periodic. Due to their ability to reflect a specific range of wavelengths, photonic crystals are used in many applications such as optical filters and waveguides [1]. Plasma photonic crystals are based on the same basic concept of solid photonic crystals because the refractive index of plasma differs from that of air. Hojo and Mase [2] have developed a dispersion relation for electromagnetic waves traversing one-dimensional plasma photonic crystals, but they used low density plasma ($n_e = 1 \times 10^{14}$ cm^{-3}) and they neglected the collisional frequency term when deriving the dielectric constant in plasma.

This thesis, however, will focus on the application of microplasma arrays to realizing photonic crystals. One unique characteristic of microplasmas is an operating pressure at or beyond one atmosphere, where a pressure that is corresponds to a number density that is far too high for the collision frequency for momentum transfer (ν_m) to be ignored. Therefore, it is essential to invoke the Drude model which will lead to a complex refractive index for the plasma [3, 4]. Perhaps the greatest asset of microplasma-based photonic crystals is their ability to be reconfigured at electronic speeds, simply because all of the plasma in the array is addressable. Since plasma photonic crystals can control both periodic structure and refractive index of plasma, this research topic will be significant in many applications.

CHAPTER 2

LOW TEMPERATURE PLASMA FUNDAMENTALS

A plasma is a collection of free electrons, ions, and neutrals. Plasmas are quasi neutral (electron density, $n_e \approx$ ion density, n_i) and their fractional ionization is low (typically $\leq 1\%$). An important characteristic of low temperature plasmas is their non-equilibrium condition. Specifically, their electron temperature, ion temperature, and gas temperature are not the same [5, 6]. For microplasmas, the gas temperature, T_g, can be as low as room temperature for many applications such as biomedical equipment and ozone generation, while typical values for ion and electron temperatures are 0.1 and 1 - 5 eV, respectively [7].

The Debye length and the sheath region are two important concepts associated with a plasma. The Debye length is the minimum distance over which electric charges can be screened out. That means charges will tend to neutralized. It can be derived from Poisson's equation, which relates the electrostatic potential to an electric charge distribution and is given by

$$\nabla^2 \Phi = -\frac{\rho}{\epsilon_0} \tag{2.1}$$

where Φ is the electric potential (V), ϵ_0 is the vacuum permittivity (F/m), and ρ is the charge density (C/cm^3). Starting from Poisson's equation, the Debye length can be derived with the assumption that $n_i = n_0$ and $n_e = n_0 \cdot \exp(\Phi / kT_e)$, which results in Equation (2.1). These assumptions can be made because the ions are considered to be stationary compare to electrons.

$$\lambda_D = \sqrt{\frac{\epsilon_0 \cdot kT_e}{e \cdot n_e}} \cong 743 \cdot \sqrt{\frac{T_e(\mathrm{V})}{n_e(\mathrm{cm}^{-3})}} \ [\mathrm{cm}] \tag{2.2}$$

where kT_e is the electron temperature (eV) and e is charge on an electron (C) [5, 8]. A natural consequence of this is the sheath region between the bulk plasma and the cathode. Because electrons are repelled back into the bulk

plasma by the negatively charged cathode, a region (the sheath) containing a net positive space charge will form. Ions, accelerated toward the cathode within the sheath, will produce secondary electrons which are then propelled into bulk by that same electric field. Because a sheath region must exist in order to sustain a plasma, the size of the plasma needs to be greater than the length of the sheath. Since the length of the sheath is assumed to be 3-10 times the Debye length, the size of the plasma is limited by the Debye length [5].

$$\omega_p = \sqrt{\frac{n_e \cdot e^2}{\epsilon_0 \cdot m_e}} \cong 5.634 \times 10^4 \cdot \sqrt{n_e(\mathrm{cm}^{-3})}\ [\mathrm{Hz}] \tag{2.3}$$

The plasma frequency is a measure of the frequency of electrons that oscillate around the ions and depends on the square root of the electron density as shown in Equation (2.3) [5]. This quantity determines how the plasma responds to an incident electromagnetic wave. The plasma frequency can be derived from the Drude model expression [9]:

$$m_e \frac{\partial^2 x}{\partial t^2} + m_e \nu_m \frac{\partial x}{\partial t} = -qE(t) \tag{2.4}$$

where m_e is the mass of an electron (kg) and ν_m is the electron-neutral collisional frequency for momentum transfer (Hz) which represents the rate at which an electron collides with ions. The collisional frequency is pressure dependent and it is known to be $\nu_m \cong 10^9 \cdot P$ (Torr) [6]. In a microplasma, electron densities as large as 10^{17} cm^{-3} have been measured, which corresponds to $\lambda = 2$ μm [10]. Because the Debye length is inversely proportional to the square root of the electron density, a higher electron density will give a shorter Debye length, allowing for the generation of plasma in a physically smaller geometry.

CHAPTER 3

REFRACTIVE INDEX OF MICROPLASMA

Since an index contrast between two different periodically spaced dielectric materials is the main concept behind photonic crystals, calculating the plasma refractive index as a function of the frequency of the electromagnetic wave is essential. The refractive index of a material is given by the square root of the product of the relative permittivity and the relative permeability. The relative permeability can be assumed to be 1, since a plasma is a non-magnetized material, and the relative permittivity can be derived using the Drude model [9]. According to the Drude model, the dielectric constant of a plasma depends on the plasma frequency, the incident electromagnetic wave frequency, and the collisional frequency, and is given by

$$\epsilon_p(\omega) = 1 - \frac{\omega_p^2}{\omega^2 \cdot (1 + i \cdot \frac{\nu_m}{\omega})} = \epsilon_p' + i \cdot \epsilon_p'' \tag{3.1}$$

In a conventional plasma, the collisional frequency term is often neglected since $\nu_m \ll \omega$. This results in a real ϵ_p. However, this term is not negligible in the case of a microplasma, due to its high operating pressure ($P \cong 0.1 - 1$ atm). Because the collisional frequency is not negligible in the case of a microplasma, the dielectric constant becomes complex [3]. Since $n = \sqrt{\epsilon_r \mu_r} = \sqrt{\epsilon_r}$, n is then also complex in the case of a microplasma.

$$n_p(\omega) = \sqrt{\epsilon_p(\omega)} = n_p' + i \cdot n_p'' \tag{3.2}$$

The refractive index of plasma, a complex number, can be written in complex form as shown in Equation (3.2). Here n_p' is the typical refractive index of the plasma, while n_p'' gives the absorption of the plasma. The absorption coefficient can be calculated from refractive index according to $\alpha(\omega) = 4\pi \cdot n_p''/\lambda$ [9].

Figure 3.1 is a plot of the refractive index of the plasma as a function of frequency. The positive portion of Figure 3.1 is the real part of refrac-

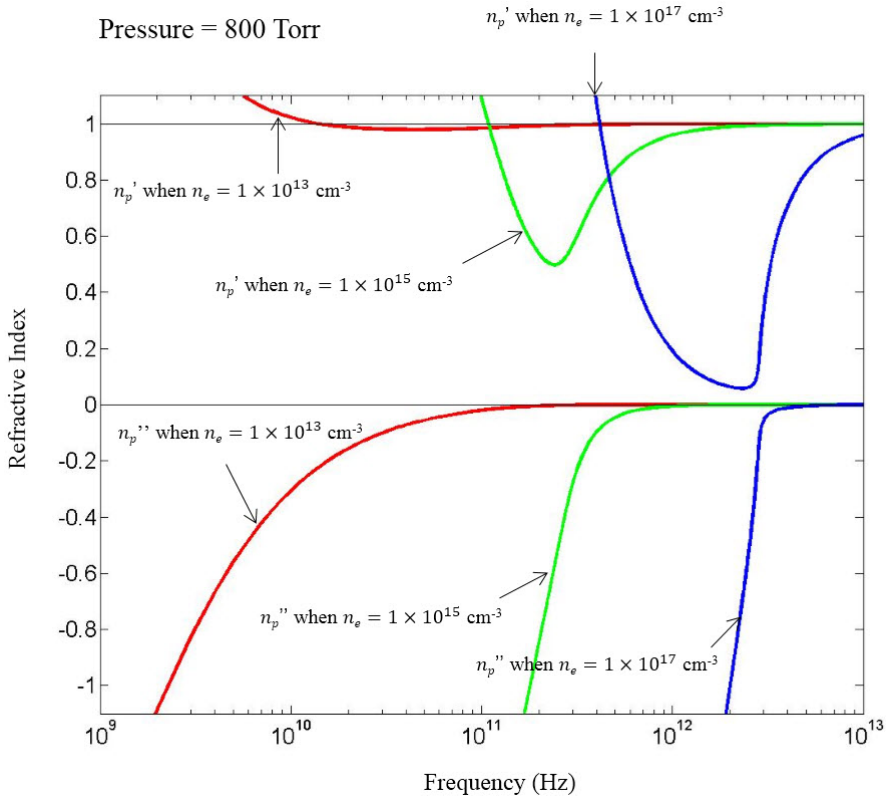

Figure 3.1: Refractive index depends on electron density and wavelength

tive index (n_p'), while the negative portion is the magnitude of the imaginary part of the refractive index (n_p''). Near the plasma frequency ($\omega \cong \omega_p$), there exists a range of frequencies that will have both a refractive index that is sufficiently different from that of air and an absorption coefficient that is sufficiently close to zero such that photonic crystals can be made.

CHAPTER 4

PREVIOUS WORK

This research is a collaboration with Professor Sakai at the University of Kyoto in Japan. Professor Sakai is one of the leading pioneers of plasma photonic crystals and has extensively tested the plasma photonic crystals shown in Figure 4.1, which have a lattice constant of 2.5 mm [3]. The working frequency of this photonic crystals ($\sim$ 60 GHz) can be calculated easily through Bragg frequency, $\nu_B = c/(2 \cdot a)$ where a is the lattice constant, and a plot of the working frequency as a function of the lattice constant is shown in Figure 4.2 (c) [1, 11]. Sakaguchi et al. also tested the dependence of transmittance on the applied voltage and pressure. A higher reflectance was measured with higher applied voltages, largely due to an increase in electron density. This is because the real part of the relative permittivity decreases as the plasma frequency increases (with increasing electron density). Also examined experimentally was the effect of the gas pressure. Lower transmittance was measured with lower pressures, because a lower pressure correspond to a lower collisional frequency, which in turn corresponds to a decrease in the real part of the relative permittivity. Thus, as higher voltages and lower pressures are applied, the real part of refractive index gets lower, which results in a higher index contrast and a lower transmittance [3, 11].

Another device with a lattice constant of 1.5 mm was tested in Prof. Sakai's group. As expected from the Bragg frequency, waves were reflected at $\sim$ 100 GHz. However, a minimum transmittance of more than 85% was measured, a figure which was largely due to limits imposed by the fabrication of the device. There are two primary reasons for such a low reflectance. First, the boundary between the plasma and the air was not well defined, such that the periodicity of the photonic crystals could not be determined clearly (see Figure 4.2 (a)) [11]. Second, the real part of refractive index at 100 GHz is almost 1 which is almost the same as that of air with electron density of 1×10^{13} cm^{-3}. For a working frequency of 100 GHz and beyond, devices

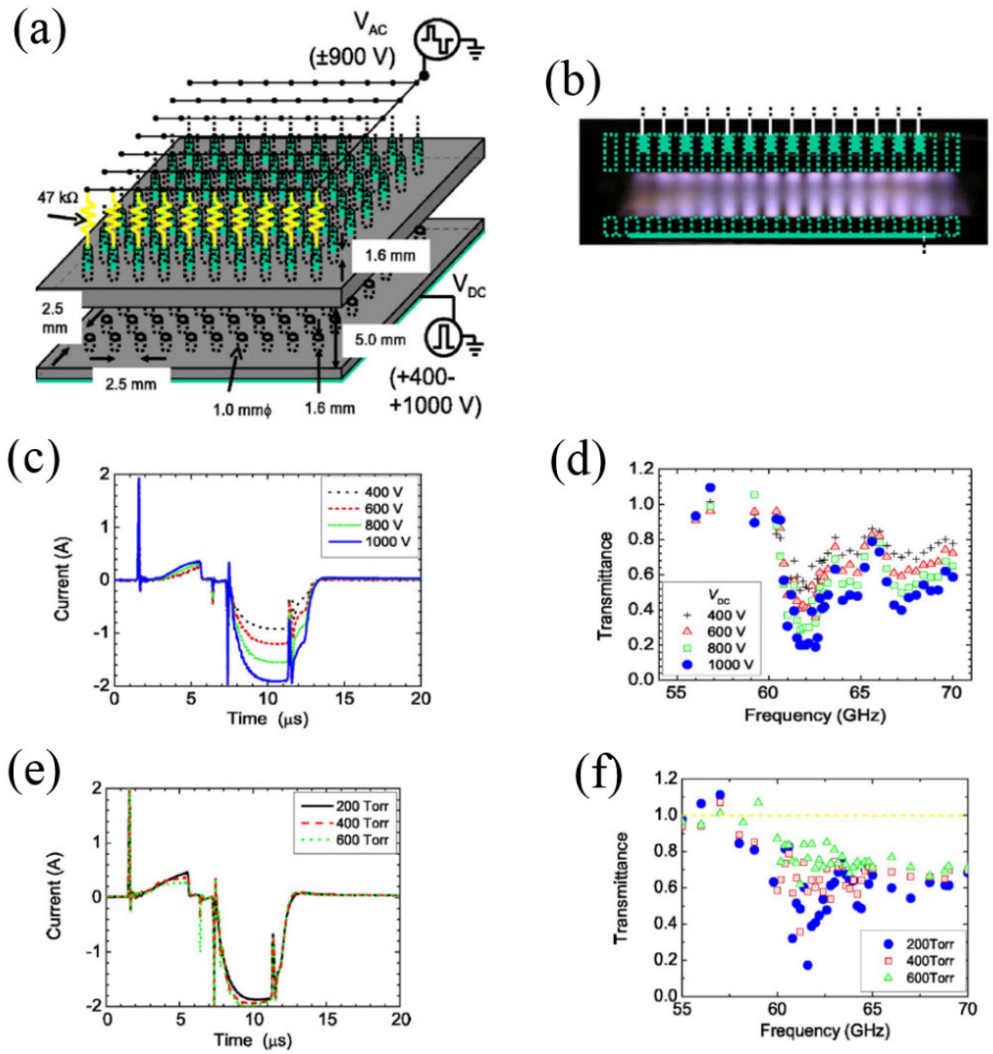

Figure 4.1: Device diagram and discharging image with a = 2.5 mm, transmittance with different voltage and pressure [11]

with higher electron densities are required. The devices developed here at the University of Illinois, and discussed in the Chapter 5, have higher electron densities and much clearer boundaries between the microplasma and the air, enabling a wider range of working frequency to be covered [3].

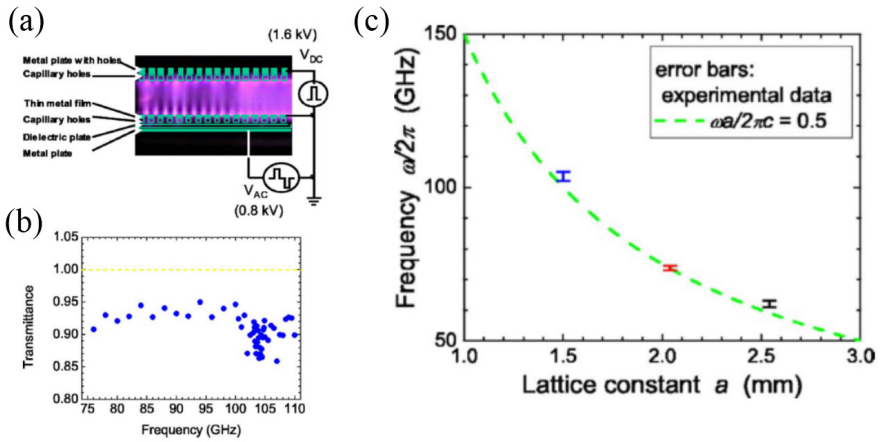

Figure 4.2: (a) Discharging image, (b) transmittance with $a = 1.5$ mm and (c) working frequency plot [11]

CHAPTER 5

1-D AND 2-D PLASMA PHOTONIC CRYSTALS

Devices suitable for use as 1-D and 2-D plasma photonic crystals have been fabricated and demonstrated to discharge. For 1-D plasma photonic crystals, a device made of Al (aluminum) and nanoporous Al_2O_3 (alumina) has been fabricated.

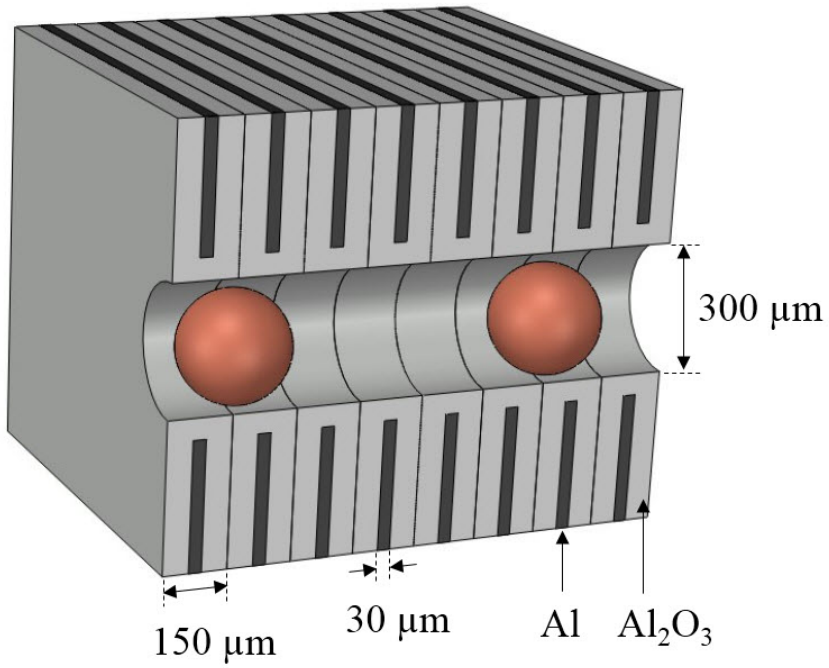

Figure 5.1: Cross-sectional diagram for 1-D plasma photonic crystals

Many Al/Al_2O_3 electrodes are stacked together so that the position of the plasma can be controlled by selectively applying voltage to two or more consecutive electrodes as shown in Figure 5.1. Operating devices, shown in Figure 5.2, are a stack of two electrodes, however devices with

a greater number of stacks can be fabricated in the future. These devices were operating in 500 Torr of Ne gas and exhibited an ignition voltage of $\sim 200\ V_{RMS}$ (under a 20 kHz sinusoidal driving waveform).

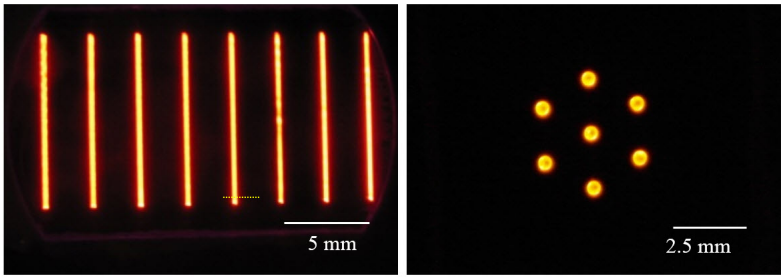

Figure 5.2: Images of plasma generated in both microchannels (left) and microcavities (right) in 500 Torr of Ne gas

For 2-D plasma photonic crystals, arrays of microplasma jets will be used to produce arrays of plasma columns. These devices, illustrated in Figure 5.3, are made of room temperature vulcanization (RTV) silicone and copper wires.

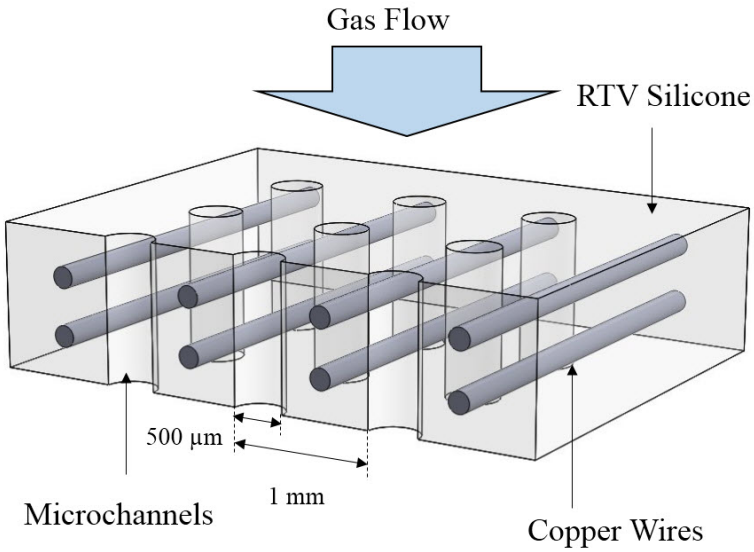

Figure 5.3: Cross-sectional diagram for 2-D plasma photonic crystals

Helium gas, at a backing pressure of 760 - 900 Torr, will flow through the array of microchannels embedded in the RTV silicone. Plasma

will be generated within these microchannels before being subsequently ejected into the air. Figure 5.4 shows a device operating in He gas at 2.5 $kV_{pk\text{-}pk}$ (20 kHz sinusoidal driving waveform). The length of the plasma jet is $\sim$ 2 mm, and can be extended by placing an extra electrode near the edge of the plasma jet. It is possible to extend this length up to at least 5 mm, as shown in Figure 5.4 (right).

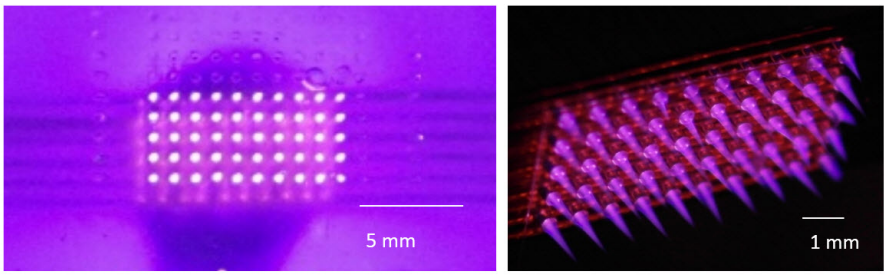

Figure 5.4: Top (left) and perspective (right) view of a microplasma jet array

CHAPTER 6

EXPERMENTAL SETUP

The experimental setup for plasma photonic crystals is shown in Figure 6.1. The period of 2-D plasma jet arrays is 1 mm and this corresponds to the working frequency region of 150 GHz according to the Bragg frequency plot in Figure 4.2. The microwave will be generated from a signal generator (E8257D-520, Keysight Technologies). Because this signal generator can only generate a frequency range up to 20 GHz, this wave will be multiplied by 8 times (up to 170 GHz) through a signal generator extension module (WR6.5 AMC, Virginia Diodes Inc.). The wave from the frequency multiplier that will propagate through the plasma photonic crystals will be detected by a spectrum analyzer (PXA Signal Analyzer N9030A, Keysight Technologies) through frequency mixer (WR6.5 MixAMC, Virginia Diodes Inc.) that divides wave frequency by factor of 8. A frequency mixer, comprised of spectrum analyzer extension modules, is required to detect the frequency range around 150 GHz because the spectrum analyzer can only detect signals up to 26.5 GHz.

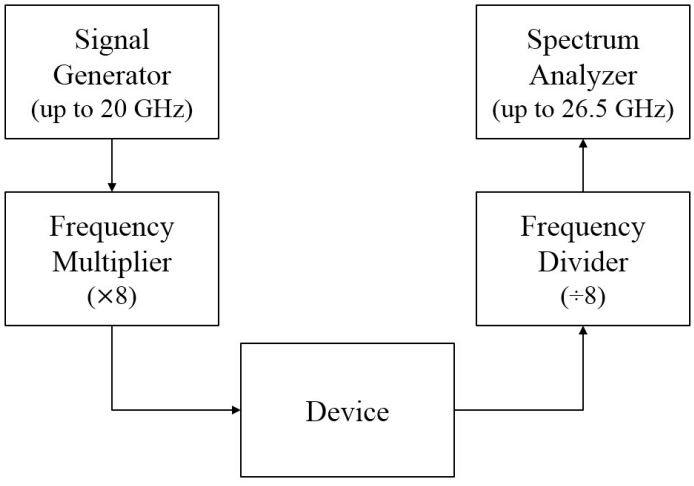

Figure 6.1: Experimental setup for plasma photonic crystals

CHAPTER 7

SIMULATION

Equipment has been ordered to test a microwave transmission through plasma photonic crystals. Because the equipment has not arrived yet, this thesis will contain simulation data derived through finite-difference time-domain (FDTD) software called *Lumerical*. A refractive index of plasma from the software between 100 GHz and 200 GHz has been compared with that from the Drude model.

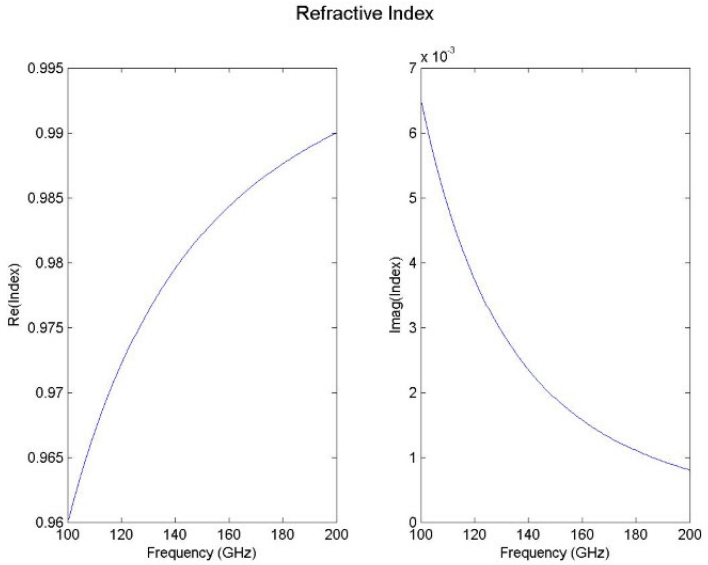

Figure 7.1: Refractive index of plasma from the Drude model

In Figures 7.1 and 7.2, the real part of refractive index (left), n_p', and the imaginary part of refractive index (right), n_p'' of plasma are exactly the same for both the Drude model and *Lumerical* experiment. The results confirm that simulation data from *Lumerical* is trustworthy since the refractive index of plasma from *Lumerical* is derived from the Drude model.

The device structure is shown in Figure 7.3 with gray-colored columns that represent plasmas. The device has 10 by 10 columns; period

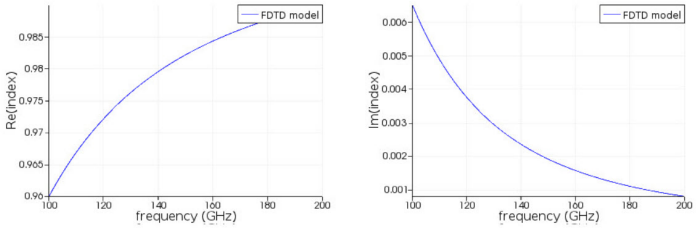

Figure 7.2: Refractive index of plasma from *Lumerical*

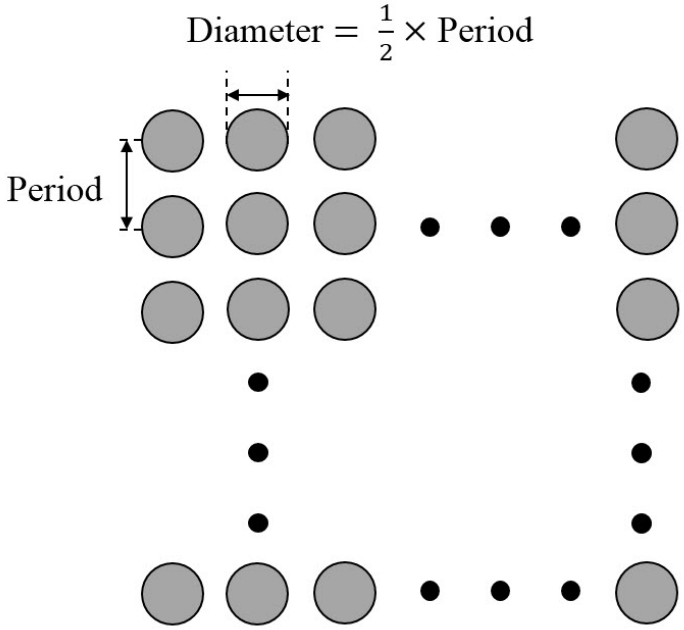

Figure 7.3: Device structure on simulation

is 1 mm and the diameter of each column is 500 μm. The top and bottom sidewalls are set to periodic and the left and right sidewalls are set to perfectly matched layer (PML) that has no electric field or magnetic field. The plane wave is generated on the left sidewall and the detector is placed at the right sidewall. Because Bragg frequency for a period of 1 mm is 150 GHz, the frequency of the plane wave is increased from 100 GHz to 200 GHz.

Figures 7.4, 7.5, and 7.6 have two plots on the left that show the real part and the imaginary part of the refractive index of plasma according to the wave frequency with an electron density of $n_e = 1 \times 10^{14}$ cm^{-3} and collisional frequency of $\nu_m = 0$, 1×10^{10}, and 1×10^{11} Hz, respectively. Since ν_m (Hz) $\cong 10^9 \cdot P$ (Torr), this corresponds to the gas pressure of 0, 10, and 100 Torr. Plots on the right show wave transmission through plasma photonic

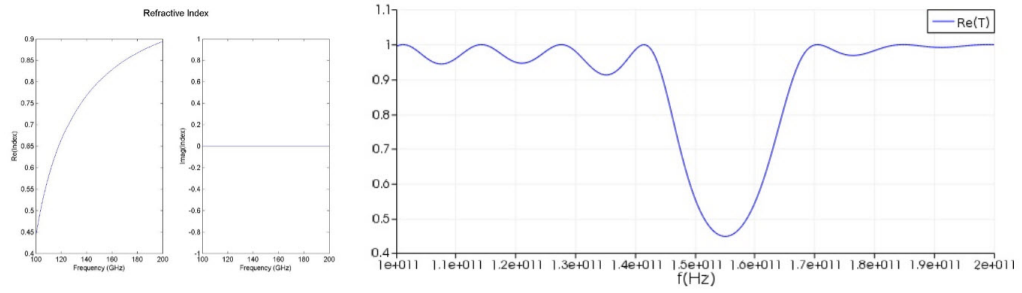

Figure 7.4: Refractive index of plasma (left) and wave transmission with $n_e = 1 \times 10^{14}$ cm^{-3} and $\nu_m = 0$ Hz (right)

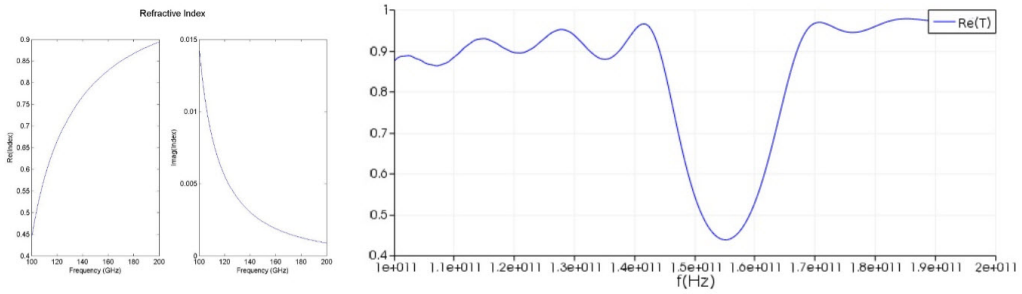

Figure 7.5: Refractive index of plasma (left) and wave transmission with $n_e = 1 \times 10^{14}$ cm^{-3} and $\nu_m = 1 \times 10^{10}$ Hz (right)

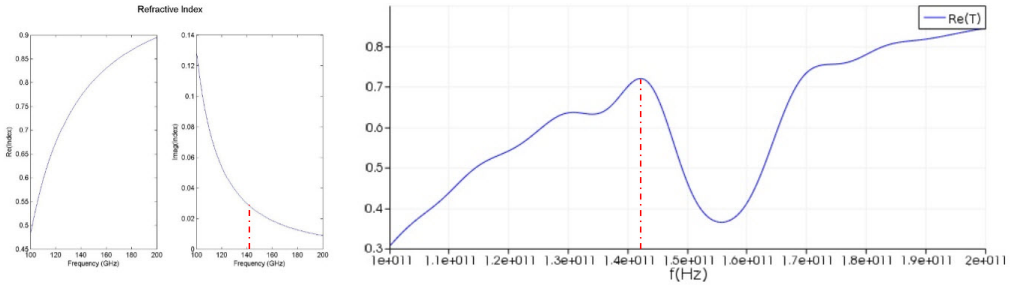

Figure 7.6: Refractive index of plasma (left) and wave transmission with $n_e = 1 \times 10^{14}$ cm^{-3} and $\nu_m = 1 \times 10^{11}$ Hz (right)

crystals; there is reflection around 150 GHz.

The transmission plot from the simulation through plasma condition with $n_e = 1 \times 10^{14}$ cm^{-3} and $\nu_m = 0$ Hz is shown in Figure 7.4. The imaginary part of the refractive index of plasma is zero because this is the same as the collisionless plasma case. When the refractive index of plasma only has a real part with zero imaginary parts, there is no attenuation of the wave when the wave propagates through plasma. Transmittance of the wave

had decreased down to $\sim 40\%$ around 150 GHz and near 100% on the other frequency regions.

In Figure 7.5, the electron density was kept the same but the collisional frequency was $\nu_m = 1 \times 10^{10}$ Hz. This collisional frequency term caused the imaginary part to be non-zero but the transmission has the same trend as the collisionless case. When the collisional frequency has increased to 1×10^{11} Hz, the transmittance was almost the same except for the lower frequency region where it decreased to less than 10%. Figure 7.6 shows the transmittance plot when $n_e = 1 \times 10^{14}$ cm^{-3} and $\nu_m = 1 \times 10^{11}$ Hz and this corresponds to 100 Torr of the gas. Wave transmittance decreased for the lower frequency region because the lower frequency has a higher imaginary part of the refractive index. It seems that transmittance is acceptable when frequency is greater than ~ 142 GHz and has an imaginary part of ~ 0.03. Therefore, the imaginary part of the refractive index should be less than 0.03 in order to avoid wave attenuation by plasma.

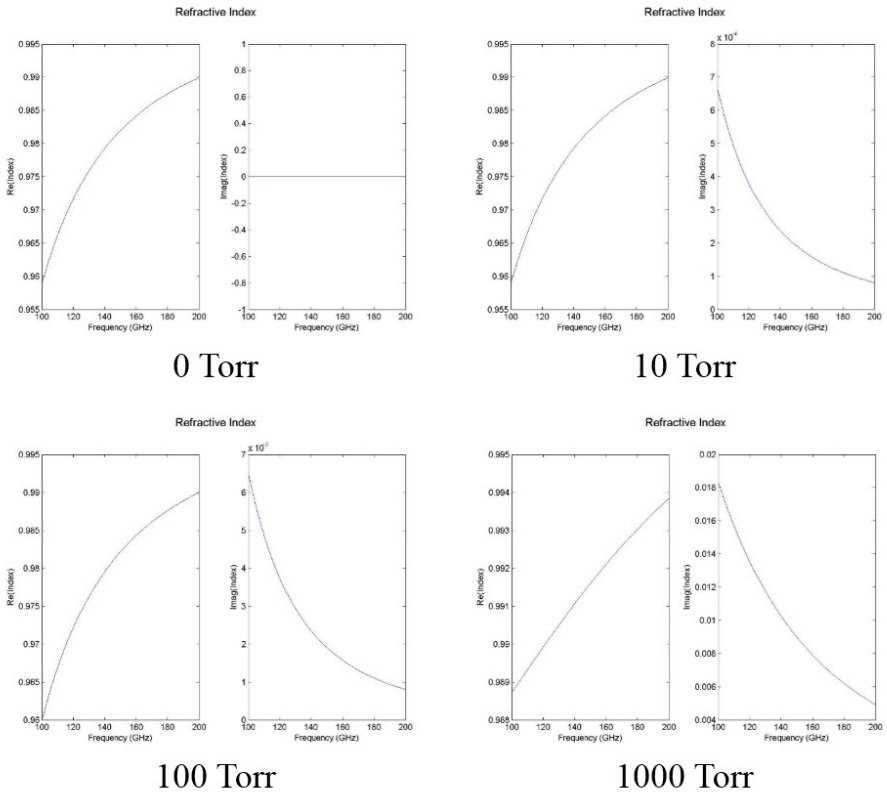

Figure 7.7: Refractive index and transmission with $n_e = 1 \times 10^{13}$ cm^{-3}

To avoid attenuation of the wave, a lower imaginary part for the

refractive index is required. Because lower electron density causes lowering of the imaginary part of the refractive index, the refractive index of plasma is plotted in Figure 7.7 with pressures of gas of 0, 10, 100, and 1000 Torr. The imaginary part is always much less than 0.03, so there would not be much attenuation of the wave by plasma.

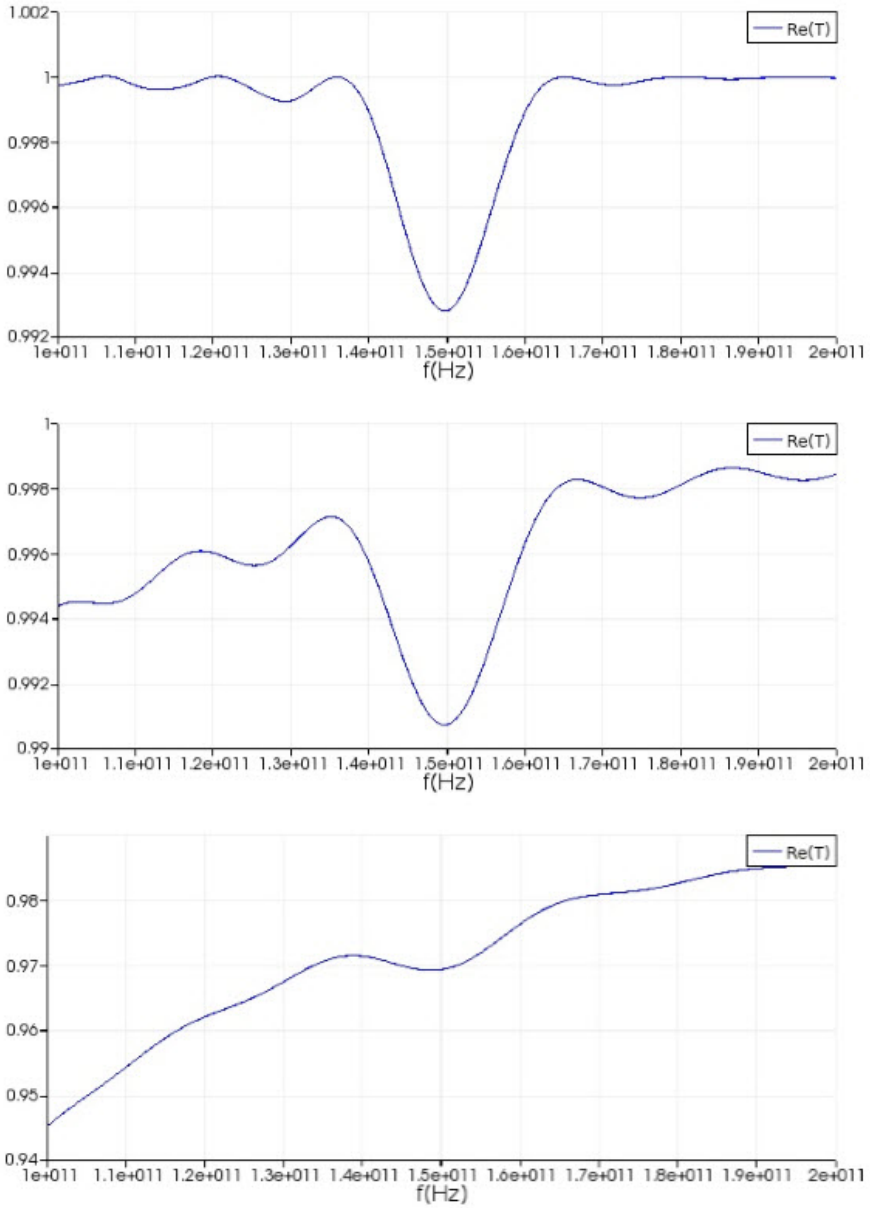

Figure 7.8: Transmission with $\nu_m = 0$ Hz (top), 1×10^{10} Hz (middle), 1×10^{11} Hz (bottom)

In Figure 7.8, the transmittance plots show that there is not much

attenuation but also there is not enough reflection of wave at 150 GHz. Because the real part of the refractive index is too close to 1 that is index of air, it is hard to see the effect of photonic crystals. This means that the real part of the refractive index of plasma should be less than 0.9 to see the effect of photonic crystals.

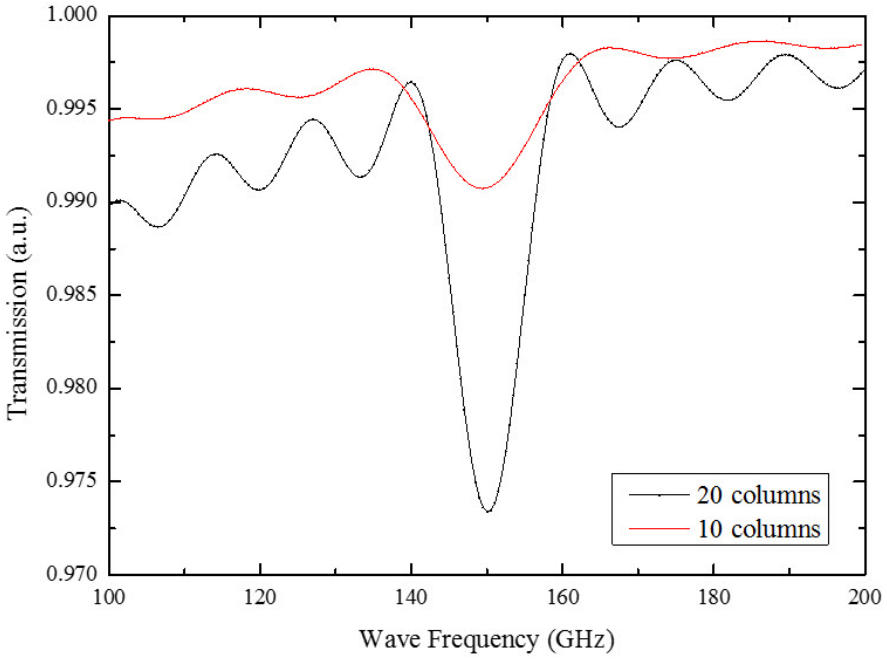

Figure 7.9: Transmission with different numbers of plasma columns

Another way of lowering the reflection at Bragg frequency is to change the number of plasma columns in the plasma photonic crystals. In the case of $n_e = 1 \times 10^{13}$ cm^{-3} and $\nu_m = 1 \times 10^{10}$ Hz, transmittance was simulated with both 10 columns and 20 columns as shown in Figure 7.9. For 20 plasma columns, overall transmittance was decreased since there is more plasma to propagate through, however, reflection at around 150 GHz has increased significantly. More columns also helps the plasma columns to work as photonic crystals.

CHAPTER 8

CONCLUSION AND FUTURE WORKS

Since arrays of microplasma jets have well-defined plasma-air boundaries and electron densities which are high enough to reflect waves with a frequency higher than 100 GHz, they are expected to achieve control over a much wider portion of the electromagnetic spectrum than previously demonstrated by the plasma photonic crystals. Photonic crystals comprising arrays of microplasmas can serve as reconfigurable filters in the GHz-THz spectral region.

As soon as equipment is available, devices for the plasma photonic crystals will be tested and checked in simulations with corresponding electron density and collisional frequency. It is important to find the proper electron density and collisional frequency to have the real part of the refractive index of plasma to be less than 0.9 and the imaginary part of the refractive index of the plasma that is less than 0.03 for plasma photonic crystals to work well.

REFERENCES

[1] B. E. A. Saleh and M. C. Teich, *Fundamentals of Photonics*, Wiley-Interscience, New York, NY, 1991.

[2] H. Hojo and A. Mase, "Dispersion relation of electromagnetic waves in one-dimensional plasma photonic crystals," *J. Plasma Fusion Res.*, vol. 80, no. 2, pp. 89-90, 2004.

[3] O. Sakai, T. Sakaguchi, Y. Ito, and K. Tachibana, "Interaction and control of millimetre-waves with microplasma arrays," *J. Plasma Fusion Res.*, vol. 47, no. 12B, pp. B617-B627, 2005

[4] O. Sakai and K. Tachibana, "Properties of electromagnetic wave propagation emerging in 2-D periodic plasma structures," *IEEE Trans. Plasma Sci.*, vol. 35, no. 5, pp. 1267-1273, 2007.

[5] M. A. Lieberman and A. J. Lichtenberg, *Principle of Plasma Discharges and Material Processing*, Wiley-Interscience, New York, NY, 2005.

[6] A. Fridman and L. A. Kennedy, *Plasma Physics and Engineering*, CRC Press, Boca Raton, FL, 2004.

[7] M. H. Kim, J. H. Cho, S. B. Ban, R. Y. Choi, E. J. Kwon, S.-J. Park, and J. G. Eden, "Efficient generation of ozone in arrays of microchannel plasmas," *J. Phys. D. Appl. Phys.*, vol. 46, p. 305201, 2013.

[8] B. E. Cherrington, *Gaseous Electronics and Gas Lasers*, Pergamon Press, Elmsford, NY, 1979.

[9] S. L. Chuang, *Physics of Photonic Devcies*, Wiley & Sons, Hoboken, NJ, 2009.

[10] D. Yarmolich, Y. E. Krasik, E. Stambulchik, V. Bernshtam, J. K. Yoon, B. Herrera, S.-J. Park, and J. G. Eden, "Self-pulsing 10^4 A cm^{-2} current density discharges in dielectric barrier Al/Al_2O_3 microplasma devices," *Appl. Phys. Lett.*, vol. 94, p. 011501, 2009.

[11] T. Sakaguchi, O. Sakai, and K. Tachibana, "Photonic bands in two-dimensional microplasma arrays. II. Band gaps observed in millimeter and subterahertz ranges," *J. Appl. Phys.*, vol. 101, no. 7, p. 073305, 2007.